THE ASTROPHYSICAL JOURNAL, 537:433–447, 2000 July 1

A MULTIWAVELENGTH CAMPAIGN ON γ CASSIOPEIAE. IV. THE CASE FOR ILLUMINATED DISK-ENHANCED WIND STREAMS

STEVEN R. CRANMER,[1] MYRON A. SMITH,[2] AND RICHARD D. ROBINSON[3]
Received 1999 September 12; accepted 2000 February 8

ABSTRACT

On 1996 March 14–15 we conducted a campaign with the *Hubble Space Telescope* GHRS to observe the Si IV $\lambda\lambda$1394, 1403 lines of the B0.5e star γ Cas at high temporal and spectral resolution. As a part of this $\sim$22 hr campaign, the *Rossi X-Ray Timing Explorer* (*RXTE*) was also used to monitor this star's copious and variable X-ray emission. In this fourth paper of a series we present an analysis of the rapid variations of the discrete absorption components (DACs) of the Si IV doublet. The DACs attain a maximum absorption at -1280 km s^{-1}, taper at higher velocities, and extend to -1800 km s^{-1}. The DACs in this star's resonance lines have been shown to be correlated with a $\gtrsim$6 yr cycle in the Balmer line emission V/R ratio, and in 1996 this DAC strength was near its maximum. We derive hydrogen densities of 10^9–10^{10} cm^{-3} in the DAC material using a curve-of-growth method and find that the plasma becomes marginally optically thick near -1280 km s^{-1}. The "mean DAC" probably represents a broad "plateau" with a volume density intermediate between the star's midlatitude wind and equatorial disk. We also follow the blueward evolution of subfeatures in the DACs. These features appear to emanate primarily from one or two discrete azimuths on the star and accelerate much more slowly than expected for the background wind, thereby exhibiting an enhanced opacity spiral stream pattern embedded within the structure forming the DAC. In the first two papers in this series, we suggested that active X-ray centers are associated with at least two major cool clouds forced into corotation. Several correlations of flickering in the Si IV DACs are found in our data, which support the idea that changes in X-ray ionizing flux cause changes in the ionization of material at various sectors along the spiral pattern. We demonstrate that similar flickering is visible in archival *IUE* data from 1982 and may also be responsible for earlier reports from *Copernicus* of rapid changes in this star's UV and optical lines. Finally, we discovered that flickering of the DAC fluxes in the 1982 data is correlated with rotation phase and shows a modulation with a 7.5 hr cyclical cessation of X-ray flares that was observed recently by *RXTE*. This confirms our basic picture that lulls in X-ray activity close to the star's surface cause both a lower Si V ionization fraction and an increase in Si IV variability within the DAC structures.

Subject headings: circumstellar matter — line: profiles — stars: early-type — stars: emission-line, Be — stars: individual (γ Cassiopeiae) — stars: winds, outflows

1. INTRODUCTION

The bright star γ Cassiopeiae (B0.5 IVe, HD 5394) was the first known classical Be star (Secchi 1867). Struve (1931) first suggested that the strong Balmer emission lines that characterize the Be phenomenon arise because of a rotationally flattened circumstellar envelope. This insight continues even now to guide the interpretation of observations. More is known about γ Cas than about most other Be stars, first because of its long history of observation, and second because it has been detected easily in radio (Taylor et al. 1990) and X-ray (Mason, White, & Sanford 1976) wavelengths. The history of measurements in the optical, ultraviolet, and X-ray regions has been reviewed by Doazan (1982) and Horaguchi et al. (1994).

In addition, γ Cas has been well studied because it is known to have several types of variable circumstellar structures, two of which occur commonly around Be stars. The first of these is a circumstellar decretion disk which was formed—in its present guise—in the 1930s (see Doazan 1982). This disk has been imaged in Hα to at least 6 R_* by a few groups (e.g., Mourard et al. 1989; Quirrenbach et al. 1997), giving rise to an estimated aspect angle $i \approx 45°$. This disk is well known to exhibit a cyclical violet-to-red (V/R) variation in the double-peaked Balmer emission lines (e.g., Doazan 1982; Telting & Kaper 1994). It is now widely accepted that these variations are caused by the development of a one-armed density oscillation in the disk that precesses around the star with a several year period (Okazaki 1991, 1997; Papaloizou, Savonije, & Henrichs 1992). A combination of interferometry and kinematic data from the Hα line have been used recently to map the precession of the one-armed perturbation over the last several years (Berio et al. 1999).

The second of the two commonly occurring Be star–related phenomena that is also exhibited by γ Cas is a supersonic stellar wind (e.g., Henrichs et al. 1983; Lamers & Waters 1987; Telting & Kaper 1994). Statistical studies indicate that such winds are most visible in ultraviolet spectra for Be stars viewed at intermediate latitudes (Grady, Bjorkman, & Snow 1987), and these winds frequently exhibit azimuthal asymmetries (Peters 1998). The time-dependent nature of the wind from γ Cas will form an important part of this paper.

Complex interactions between the stellar wind, disk, and other structures around γ Cas are evidenced by spectral variability observed on timescales of hours to decades. In

[1] Harvard-Smithsonian Center for Astrophysics, Cambridge, MA 02138.
[2] STScI/CSC, Space Telescope Science Institute, 3700 San Martin Drive, Baltimore, MD 21218.
[3] Catholic University of America; and LASP, Goddard Space Flight Center, Greenbelt, MD 20771.

this paper we continue the analysis of a multiwavelength observational campaign undertaken in 1996 March to monitor γ Cas over about one rotational cycle. The program data include (1) rapid time series spectra of the Si IV $\lambda\lambda$1394, 1403 lines, obtained with the Goddard High Resolution Spectrograph (GHRS) on board the *Hubble Space Telescope*; (2) high-dispersion ultraviolet echellegram spectra from 1150 to 1950 Å, obtained with the Short Wavelength Prime (SWP) camera on the *International Ultraviolet Explorer* (*IUE*); and (3) X-ray flux measurements in the 2–15 keV range, made with the Proportional Counter Array on the *Rossi X-Ray Timing Explorer* (*RXTE*) satellite. Data sets (1) and (3) were taken simultaneously on 1996 March 14–15, and data set (2) was taken on 1996 January 18–19. Archival ultraviolet spectra of γ Cas from *IUE* (1982) and *Copernicus* (1977) are also examined to obtain a more comprehensive view of the circumstellar variability.

The first three papers of this series have established that most of the ultraviolet variability can be understood in terms of corotating circumstellar structures and the occultation of active X-ray centers distributed both on the stellar surface and in overlying regions. In Paper I (Smith, Robinson, & Corbet 1998a) the basal X-ray emission was found to anticorrelate with the GHRS ultraviolet continuum variations, suggesting rotational modulation of hot ($\sim 10^8$ K) surface sites with a period of 1.123 days. Also, the occurrence of flarelike X-ray "shots" distinguishes γ Cas from most other Be/X-ray stars (predominantly binaries) and leads to a picture of unstable magnetic loops emerging from the photosphere (see also Smith 1995).

In Paper II (Smith, Robinson, & Hatzes 1998b), the analysis of the GHRS and *IUE* continuum light curves led to the suggestion that at least two large (~ 0.1–$1\ R_*$) clouds of relatively cool (~ 7000 K) plasma corotate above the surface of the star. Both the short durations of light-curve minima (in the ultraviolet continuum flux) and the lack of correlated Si IV line variability appear to rule out surface star spots and thus support the circumstellar "canopy" picture from Paper I. Temporal variations in the GHRS absorption lines were studied in Paper III (Smith & Robinson 1999), and additional corotating material at temperatures ranging between 7500 and 35,000 K was identified. Short-lived and optically thick "ultrasharp features" in the spectra suggest nonthermal explosive events, consistent with large-scale magnetic field instabilities and reconnection between the star and the equatorial disk.

The presence of magnetically active clouds above the photosphere is not considered a distinguishing characteristic of Be stars. However, some subset of Be stars shows evidence for this type of circumstellar structure, either ubiquitously present (Balona 1999; Balona & Kaye 1999) or of a transient nature (Štefl et al. 1998). Some of these show signatures of a cool temperature (Smith 2000), also suggesting a magnetic origin. Further striking examples of spectroscopically inferred magnetic material are the tilted dipolar magnetospheres of some helium-strong Bp stars (Shore & Brown 1990; Short & Bolton 1994) and the rotating spoke or spiral-like modulations around Herbig Ae/Be stars such as AB Aur (Böhm et al. 1996) and many B supergiants (e.g., Fullerton et al. 1997).

From studies of the solar wind (see, e.g., Hundhausen 1972; Burlaga 1984), it is known that regions of open magnetic field cause the flow from coronal holes to be accelerated faster than the mean ecliptic-plane wind, resulting in colliding fast and slow streams known as "corotating interaction regions" (CIRs). By extension, it is believed that several types of variable stellar spectra can arise from the passage of similar spiral CIR structures in front of the stellar disk (Mullan 1984, 1986). Cranmer & Owocki (1996) modeled the formation of CIRs in the wind of a rapidly rotating O supergiant and found that the increased opacity in these structures generated realistic discrete absorption components (DACs) in the modeled P Cygni line profiles.

Although DACs are present in the majority of O-star and Be-star ultraviolet spectra (Howarth & Prinja 1989; Grady et al. 1987), they seem to behave differently in those two types of stellar environments. The DACs in O-star spectra are often relatively weak optical depth enhancements in P Cygni absorption profiles that propagate from low to high blueshifted velocities over timescales comparable to the stellar rotation (Prinja 1988; Henrichs, Kaper, & Zwarthoed 1988). In contrast, DACs in the lines of Be stars are strong absorptions superimposed on a weak or nonexistent wind profile (not P Cygni), and they appear to remain at a constant velocity for weeks or months at a time (e.g., Henrichs et al. 1983). Moreover, when they reoccur they tend to favor a velocity range that is unique to the star.[4] Doazan et al. (1987) and Telting & Kaper (1994) found a correlation between the presence and strength of DACs in γ Cas *IUE* spectra and the above-mentioned V/R cyclical pattern in Balmer emission lines. It seems clear, then, that the winds and disks of Be stars exhibit some kind of mutual interaction. The principal goal of this paper is to use the DACs in the ultraviolet resonance lines of γ Cas to begin to determine the nature of this interaction.

The remainder of this paper is organized as follows. In § 2 we describe the GHRS spectral line observations that form the empirical basis of this work. In § 3 the Si IV DAC features are analyzed quantitatively in order to probe both the time-averaged plasma properties (§ 3.1) and the rotationally modulated wind dynamics (§§ 3.2–3.3). In § 4 we examine additional GHRS, *IUE*, and *Copernicus* data in order to obtain a more robust picture of the visibility of the circumstellar structures, and in §§ 5–6 we interpret our results in the light of a general scenario for the wind and disk properties of γ Cas.

2. GHRS OBSERVATIONS

Spectroscopy of the Si IV $\lambda\lambda$1394, 1403 doublet was obtained with the 2″ Large Science Aperture of GHRS, using its medium-resolution G160M grating. The continuum intensity of γ Cas resulted in approximately 8100 counts s^{-1} $diode^{-1}$, and the spectral resolution ($\lambda/\Delta\lambda$) was at least 10^4 in the Si IV lines. The observations began at 21:18 UT on 1996 March 14 and lasted for 13 orbits of the *Hubble Space Telescope* (*HST*), into March 15. In total, 1045 minutes of data were obtained over a 1280 minute timeline.[5] The data were binned into 1 minute averages to increase the signal-to-noise ratio, and for some of the sub-

[4] Some O-star DACs do remain at constant blueshifted velocities for many days (e.g., 15 Mon and λ Ori; see Kaper et al. 1996), but they coexist with accelerating DACs. Be stars such as γ Cas are qualitatively different in that red-to-blue acceleration has not been observed for the strong DACs.

[5] These data are archived by the MAST (Multi-Mission Archive at Space Telescope) facility and are available at the URL http://archive.stsci.edu/hst/gammacas/index.html.

sequent analysis in this paper we increased the binning to 11 minutes to improve the statistics further. Papers I and II describe the removal of instrumental effects—such as fixed pattern noise, orbital wavelength shifts, and geomagnetically induced intensity variations—from this data set.

In the central panel of Figure 1 we show the time-averaged Si IV $\lambda\lambda$1394, 1403 spectrum of γ Cas in units of a normalized ultraviolet continuum flux. The zero-velocity absorption lines are broader than the strong DACs (the latter at a blueshifted velocity of about -1280 km s^{-1}) but are of comparable equivalent width. Because the mean spectrum is used below as a normalization quantity, we have smoothed it in the spectral direction by averaging over a simple "boxcar" window function of width 0.42 Å (7 pixels). The unsmoothed average spectrum is plotted in Figure 1 of Paper II, and the only noticeable effect of the smoothing is to remove the fine structure in the core of the DACs.

In Figure 1 we have also plotted the (unsmoothed) minimum and maximum flux levels observed at each wavelength over the 1280 minute observation period. The temporal variability of the data is also indicated by the standard deviation of the normalized flux plotted in the

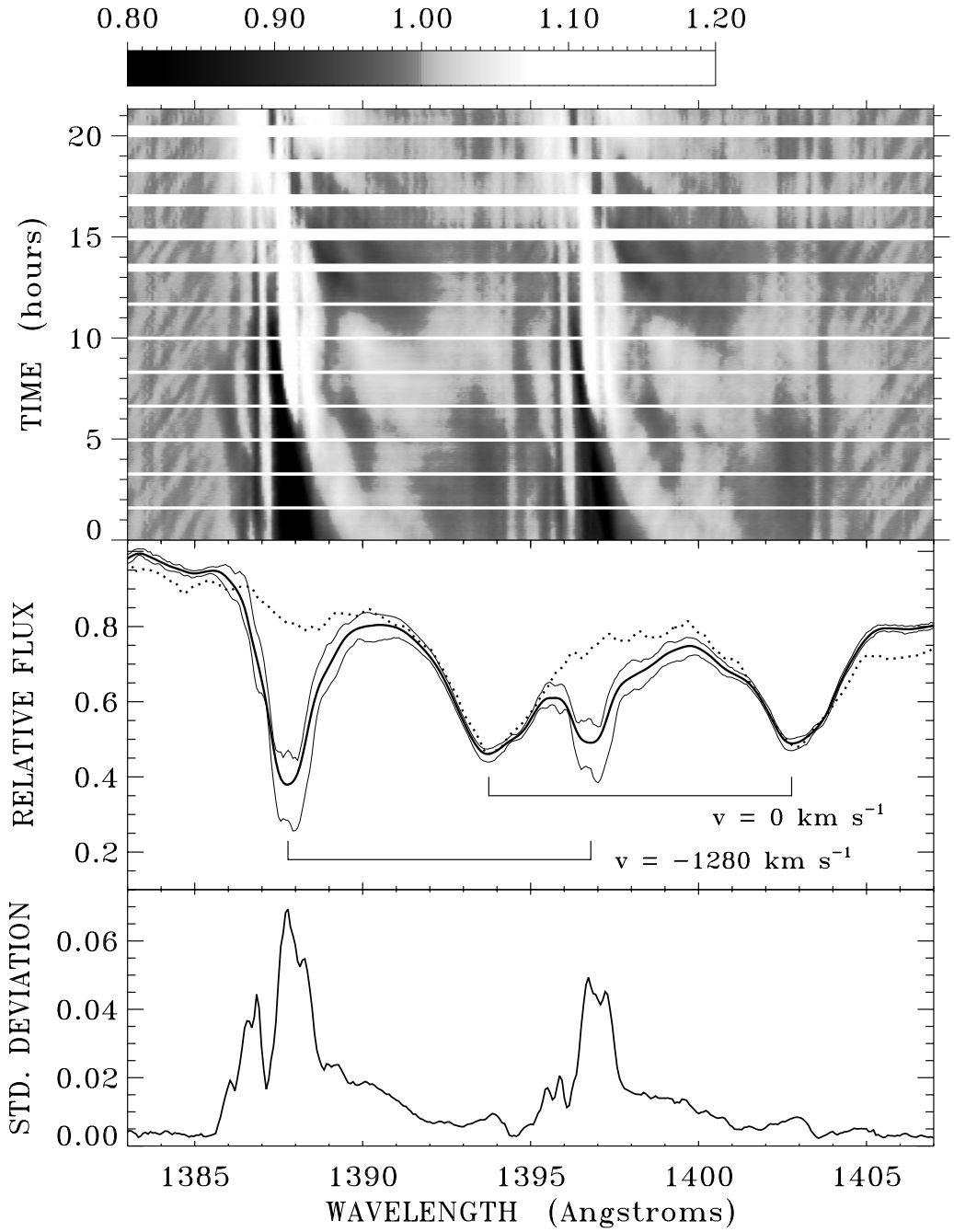

FIG. 1.—Si IV spectral variability of γ Cas in 1996. The top panel shows time variations of the line flux (divided by the time-averaged flux at each wavelength) plotted with the gray levels defined at the top. Time is normalized to the start of the GHRS observations, and horizontal white bars represent periods of no data. The central panel shows the time-averaged flux in units of a normalized continuum flux (*thick solid line*), the minimum and maximum flux levels at each wavelength for the 1996 GHRS observations (*thin solid lines*), and Telting & Kaper's (1994) γ Cas "template spectrum" for negligible DAC activity (*dotted line*). The lower panel shows the standard deviation of the GHRS flux variations vs. wavelength.

lower panel. Notice that the DACs exhibit the largest variability, but they never disappear entirely. For reference we also plot the maximum flux "template spectrum" derived by Telting & Kaper (1994), which was constructed by averaging 20 *IUE* spectra taken between 1981 and 1989 at times when γ Cas showed negligible DAC activity. The data points for the template plotted in Figure 1 were tabulated from a scanned image of Figure 2 from Telting & Kaper (1994), obtained from the NASA Astrophysics Data System (ADS).

Because the UV continuum, the low-velocity Si IV variability (i.e., velocities more positive than $-v \sin i$), and the non–Si IV features were analyzed at length in Papers II and III, we focus mainly on the Si IV DACs in the remainder of this paper. At the top of Figure 1 is a gray-scale representation of the temporal variability of the GHRS data, centered on the Si IV doublet. The fluxes at each wavelength and time have been divided by the averaged spectrum plotted in the central panel (compare with Fig. 1*a* of Paper III, which was normalized by the continuum flux). Although the DACs as a whole represent a strong and persistent increase in the Si IV wind opacity, the variability within the DACs may denote features with either a higher or lower opacity than the "time-steady" profile. Thus, the gray scale in Figure 1 highlights these variations with respect to the time-averaged DAC profile to limit any possible bias of interpretation. These variations are primarily red-to-blue motions, indicating outward accelerations in the scattering column in front of the star; this is similar to what is commonly observed in the DACs of other O- and B-type stars (see, e.g., Kaper et al. 1996, 1999).

3. ANALYSIS OF GHRS Si IV DAC PROFILES

As summarized in § 1, Be-star DACs have been observed to vary in a manner distinct from O-star DACs. For the GHRS observations discussed in § 2, the Si IV DACs of γ Cas exhibit significant variability in strength, but as a whole the DAC absorptions do not drift in wavelength or disappear altogether over the 21 hr timeline. However, as noted above, the weaker intensity modulations within the DAC do seem to accelerate out with the stellar wind. Thus, it may be useful to examine separately the time-averaged DACs (§ 3.1) and their internal variations (§§ 3.2–3.3) and then attempt to synthesize a coherent picture of the circumstellar structures that give rise to these spectral features.

3.1. *Time-averaged DAC Density*

In order to determine the physical properties of the plasma giving rise to the mean DAC absorptions, one must make certain assumptions about its geometric and dynamical properties. Because the DACs exist at large blueshifted velocities, we make the standard assumption that they arise from the scattering of photons in the supersonic wind out of the occulting volume in front of the stellar disk, caused by a "slab" of finite extent. In a rapidly accelerating wind, an increase in the line opacity can be caused by an increased density, a larger ionization fraction, or a smaller radial velocity gradient (see, e.g., Prinja & Howarth 1984; Massa, Prinja, & Fullerton 1995b). Each of these effects is expressible as an increased effective column density of Si IV ions. In this section we estimate this empirical column density using two methods: an optically thin line-fitting procedure and a detailed curve-of-growth analysis.

3.1.1. *Optically Thin DAC Fitting*

Henrichs et al. (1983) and Telting & Kaper (1994) fit profiles of γ Cas DACs using a nonlinear χ^2 minimization algorithm, and they derived column densities assuming the features were optically thin. We duplicate this analysis in order to compare the properties of the 1996 DAC to those measured with *IUE* from 1978 to 1989. The parameterization for the relative DAC flux is

$$\frac{F(v)}{F_c(v)} = \exp\left\{-\tau_c \exp\left[-\left(\frac{v - v_c}{v_t}\right)^2\right]\right\} \times \exp\left\{-\tau_c \frac{\lambda_2 f_2}{\lambda_1 f_1} \exp\left[-\left(\frac{v - v_c - \Delta v}{v_t}\right)^2\right]\right\}, \quad (1)$$

where $F(v)$ is the time-averaged Si IV spectrum from Figure 1, $F_c(v)$ is the effective "continuum" flux given by Telting & Kaper's (1994) template spectrum, $\Delta v = 1939.1$ km s^{-1} is the doublet separation of the two lines, and the central wavelengths and oscillator strengths are given by $\lambda_1 = 1393.755$ Å, $\lambda_2 = 1402.770$ Å, $f_1 = 0.524$, and $f_2 = 0.260$ (Verner, Verner, & Ferland 1996).

The three free parameters of this fitting method are v_c, the central DAC velocity, v_t, the $1/e$ half-width of the DAC (loosely related to a turbulent velocity; see below), and τ_c, the effective optical depth of the stronger DAC. We utilized a nonlinear Levenberg-Marquardt χ^2 minimization code to find the best-fit values of these parameters, which were $v_c = -1274$ km s^{-1}, $v_t = 200.1$ km s^{-1}, and $\tau_c = 0.733$ (with approximately $\pm 5\%$ uncertainties arising from the definition of F_c). Using the optically thin approximations given by Henrichs et al. (1983), an effective value for the column density $N_{\rm Si\,IV}$ of 1.34×10^{14} cm^{-2} was determined. Considering that our data refer to another epoch, this column density is remarkably close to the maximum value of $\sim 10^{14}$ cm^{-2} reported by Telting & Kaper (1994) for similar values of v_c.

3.1.2. *Curve-of-Growth Analysis Method*

Because the derived value of τ_c above is of order unity, the optically thin approximation for the column density must be questioned. A more accurate method of deriving the value of $N_{\rm Si\,IV}$ is to compare the equivalent widths of the DACs to modeled intensities from a curve-of-growth analysis (e.g., Mihalas 1978). For a general "reversing layer" positioned above the photosphere, the equivalent width $W_{\lambda i}$ is given by

$$\frac{W_{\lambda i}}{2\,\Delta\lambda_{\rm D}} = \int_0^\infty dx\{1 - \exp\,[-\tau_i\,H(a, x)]\}\,, \quad (2)$$

where $\Delta\lambda_{\rm D} = \lambda_i\,v_{\rm th}/c$ is the Doppler width corresponding to a most probable speed $v_{\rm th}$ (presumably containing both thermal and microturbulent components), τ_i is the central optical depth for each line of the Si IV doublet ($i = 1, 2$), and $H(a, x)$ is the standard Voigt function, normalized such that $H(0, x) = e^{-x^2}$. The Lorentzian damping constant is $a = \lambda_i^2\,\Gamma/(4\pi c\,\Delta\lambda_{\rm D})$, where we assume $\Gamma \approx 9 \times 10^8$ s^{-1}, equal to the Einstein A_{ji} rate of spontaneous emission for this transition. The optical depth τ_i is varied until agreement is found with the observed equivalent width, and the column density is determined as follows:

$$N_{\rm Si\,IV} = \frac{m_e\,c}{\pi^{1/2} e^2 f_i\,\lambda_i}\,\tau_i\,v_{\rm th}\,. \quad (3)$$

We integrated the residual fluxes (F/F_c) in the DACs to obtain equivalent widths of $W_{\lambda 1} = (0.92 \pm 0.05)$ Å and $W_{\lambda 2} = (0.67 \pm 0.10)$ Å. As above, the error limits come from uncertainties in the definition of F_c, as well as in the definitions of the DAC wavelength bounds. The curve of growth analysis can be done independently for the two Si IV DACs, but there is only one unique value of $v_{\rm th}$ that results in equal column densities for the two components. In other words, the constraint

$$\frac{\tau_1}{\tau_2} = \frac{f_1 \lambda_1}{f_2 \lambda_2} \tag{4}$$

allows $v_{\rm th}$ to be determined as a solution of the curve-of-growth equations rather than be a free parameter. We find that a most probable speed of 79 km s^{-1} satisfies equation (4). This value of $v_{\rm th}$ is consistent with the empirical DAC width of $v_t \approx 200$ km s^{-1} derived above, since optically thick absorption lines are necessarily wider than unsaturated lines (with pure Doppler cores) having the same value of $v_{\rm th}$.

The solutions for the optical depths of the two lines are $\tau_1 = 3.44$ and $\tau_2 = 1.71$, and the consistent column density is $N_{\rm Si\,IV} = 2.48 \times 10^{14}$ cm^{-2}. Repeating the analysis using the lower and upper uncertainty limits on $W_{\lambda 1}$ and $W_{\lambda 2}$, the minimum and maximum possible column densities are found to be 1.49×10^{14} and 7.58×10^{14} cm^{-2}. The stronger DAC feature is just barely optically thick (i.e., with $\tau_1 \geq 1$) over an approximate ± 100 km s^{-1} range of velocities centered on -1280 km s^{-1}. This result is consistent with the near-unity ratio of fluctuations in the 1394 and 1403 Å DACs at these velocities.

The final step in this analysis is to convert column densities of Si IV ions into local volume densities of plasma. By comparing the mean DAC densities to those expected in the polar wind and equatorial disk of γ Cas, we are then able to probe the nature and origin of the material in the DACs. The conversion between Si IV column density and, e.g., electron volume density is given by

$$N_{\rm Si\,IV} = \ell n_e \left(\frac{n_{\rm H}}{n_e}\right)\left(\frac{n_{\rm Si}}{n_{\rm H}}\right)\left(\frac{n_{\rm Si\,IV}}{n_{\rm Si}}\right), \tag{5}$$

where ℓ is the radial extent of the scattering column and n denotes number densities in cm^{-3}. Assuming hydrogen and helium mass fractions $X = 0.73$ and $Y = 0.24$, the ratio $n_{\rm H}/n_e = 0.86$ for a fully ionized plasma. The silicon elemental abundance is given by the solar photospheric value of $n_{\rm Si}/n_{\rm H} = 3.5 \times 10^{-5}$ (e.g., Grevesse & Sauval 1998). Lower and upper limits on the column depth ℓ are specified to be 0.5 R_* and r, respectively (also we adopt $R_* = 7.2\ R_\odot$; see Paper III). The lower limit for ℓ is constrained by the need for the DAC absorption "slab" to occult a significant fraction of the stellar disk, and the upper limit is simply the assumed asterocentric distance of the slab. The ionization equilibrium of silicon is computed using the quasi-Saha photoionization/radiative-recombination balance of Abbott & Lucy (1985):

$$\frac{n_{i+1}}{n_i} = \frac{2U_{i+1}}{U_i}\,\frac{T_R\,T_e^{1/2}}{n_e/W}\left(\frac{2\pi m_e k}{h^2}\right)^{3/2} e^{-\chi_i/kT_R}, \tag{6}$$

where the partition functions $U_i(T_R)$ are given by Sparks & Fischel (1971), W is the standard geometrical dilution factor,

$$W = \frac{1}{2}\left[1 - \left(1 - \frac{R_*^2}{r^2}\right)^{1/2}\right], \tag{7}$$

and χ_i is the ionization potential of stage i. We fix the brightness temperature T_R at a value of $T_{\rm eff} \approx 25{,}000$ K, and set lower and upper limits on T_e to be 8000 and 24,000 K, respectively (Millar & Marlborough 1999). The ionization balance is determined mainly by the radiation field (T_R) and is only weakly dependent on the electron temperature T_e.

3.1.3. *Curve-of-Growth Density Results*

Equations (5) and (6) are solved simultaneously by iterating between them until a consistent value of n_e is determined. Solutions for n_e are found as a function of DAC distance r, but at each distance there are a total of eight solutions computed: i.e., all 2^3 combinations of the specified lower and upper bounds on $N_{\rm Si\,IV}$, ℓ, and T_e. The resulting values of n_e/W vary slowly with distance and are of order 10^{10} cm^{-3}. The total hydrogen column densities lie between 10^{20} and 10^{23} cm^{-2}. For these limits the neutral fraction of hydrogen varies from about 10^{-6} at the star's surface to 5×10^{-8} at $r = 5\ R_*$. The ionization of silicon strongly favors Si^{4+}, and the ratio of Si^{3+} to Si ranges from 0.0005 to 0.03, depending on the distance and the modeled volume density (large distances and high densities favor more trace Si^{3+}). The corresponding ionization fraction range for Si^{2+} is 10^{-8} to 10^{-5}. For reference, the densest DAC model has an optical depth of 0.05 at the 275 Å ionization edge of Si^{3+}, meaning the DACs are transparent to Si^{3+}-ionizing radiation. However, this is not necessarily true for the equatorial disk, which has an opacity at 275 Å of order one. We will assume a medium transparent to such radiation in our discussion below on X-ray illumination of Si^{4+} in the DAC material.

In Figure 2 we plot the hydrogen number density $n_{\rm H}$ consistent with the minimum and maximum derived n_e values (out of the eight solutions) for the DACs. The radial dependence of the DAC density in Figure 2 does *not* represent an actual decrease with distance within the slab. The plotted values denote the required limits on $n_{\rm H}$ if the homogeneous slab were centered at any of the radii between 1 and 5 R_*. In Figure 2 we also plot representative γ Cas disk and wind hydrogen densities versus distance from the center of the star. The lower and upper limits for the equatorial disk are taken from the empirical studies of Stee et al. (1995) and Hummel & Hanuschik (1997), respectively. The values for the polar wind assume spherical mass flux conservation and a phenomenological velocity law for the supersonic portion of the outflow:

$$\dot{M} = 4\pi r^2 v_r\, m_{\rm H}\, n_{\rm H}/X \tag{8}$$

$$v_r = v_0 + (v_\infty - v_0)\left(1 - \frac{R_*}{r}\right)^{\beta}, \tag{9}$$

where we adopt $v_0 = 20$ km s^{-1} (a representative photospheric sound speed), $v_\infty = 1800$ km s^{-1} (see Paper III), and $\beta = 0.8$ (e.g., Pauldrach, Puls, & Kudritzki 1986). The lower and upper limits in Figure 2 are computed from mass-loss rates of 3×10^{-9} and 5×10^{-8} $M_\odot$ yr^{-1} (Lamers & Waters 1987; Stee et al. 1995).

It seems evident from Figure 2 that the outflowing gas that forms the DAC is at least an order of magnitude denser

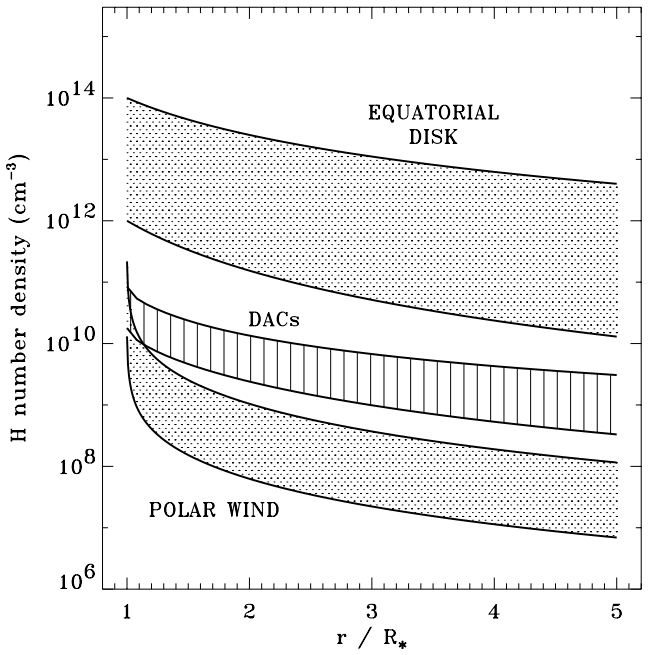

FIG. 2.—Hydrogen number density (in cm^{-3}) vs. distance. The hatched regions show lower and upper empirical limits on the number density in the dense equatorial disk (*top*) and the polar wind (*bottom*). The central region bounded by vertical lines plots the derived lower and upper limits on the number density in the time-averaged DAC as derived from the Si IV $\lambda\lambda$1394, 1403 column density. The DAC is modeled as a constant density slab at some distance r from the center of the star.

than the mean, undisturbed polar wind. However, the wind and DAC densities could be comparable to one another if the DACs are formed at $r < 1.1\ R_*$, i.e., immediately above the photosphere. The fact that the mean DACs "hover" quasi-statically at about -1280 km s^{-1} in the wind seems to rule out an origin so close to the stellar surface, though. It is also theoretically possible that the high DAC column density could be explained by a preferential ionization enhancement of Si IV or a discontinuity in the velocity gradient. Neither of these possibilities seems able to produce such a long-lasting (and rotationally invariant) opacity enhancement at a single preferred velocity in the wind.

Another possibility for the origin of the dense DAC material is the existence of compressible shocks propagating through the polar wind. However, a train of thin shocks would occupy an extremely small volume in the wind, making ℓ in equation (5) much less than R_*. The resulting number density required to produce the observed column density would thus be much larger than that plotted in Figure 2 and would also probably be much larger than theoretical predictions of shock density jumps in hot-star winds (see, e.g., Owocki, Castor, & Rybicki 1988; Feldmeier, Puls, & Pauldrach 1997). Thus, the large ℓ that allowed reasonable (order-of-magnitude) shock compressions to be considered is *incompatible* with the small ℓ also required by the shock idea. In addition, the steady state nature of the mean DAC component over many wind flow times ($t_w \approx R_*/v_\infty \sim 1$ hr) seems to preclude an origin based on propagating shocks.

Our prevailing interpretation of the time-averaged Si IV data is that the mean DAC represents a significant increase in the wind density in the occulting column in front of the star. We may imagine that as we proceed outward along any radius in the plane of our line of sight that the wind density first has a low "polar" value, then increases by roughly an order of magnitude to the DAC values shown in Figure 2, and then decreases once again by about the same amount as we move beyond the DAC-forming region. A naive application of equation (9) would place the inner edge of the plateau at about 3 R_*. Its width can vary widely between the empirical lower and upper limits on ℓ discussed above. We stress that the mean DAC structure does not seem to rotate with the star and is thus independent of the more localized spiral-shaped opacity modulations (see the following sections and Fig. 9, below) embedded within it.

3.2. *Kinematic Variability within DACs*

It is apparent from Figure 1 that the mean, time-averaged DAC analyzed above is never observed in isolation. Red-to-blue migrating flux modulations at the 10%–20% level continually propagate through (and are probably made visible by) the DAC. We applied the curve-of-growth analysis discussed in § 3.1 to these fluctuations and found a rather linear density response: changes in W_λ of $\pm 20\%$ result in changes in $n_{\rm H}$ of $\pm 26\%$. Of course, the fluctuations do not have to be caused by bulk density modulations. If, for example, the fluctuations result from a varying Si IV ionization fraction, only a $\pm 2.5\%$ change in the brightness temperature T_R is required to produce an observed $\pm 20\%$ flux variation. This effect does not strongly depend on distance from the star because n_e/W does not vary rapidly in equation (6).

In this section we perform a detailed reconnaissance of the DAC flux variations and track their temporal evolution. We primarily report on structures between 1384.0 and 1395.4 Å, or -2100 and $+350$ km s^{-1} in the 1394 Å component of the doublet. The 1403 Å component is not used because it is blended with the 1394 Å component at its most negative velocities and its fluctuations are less pronounced.

3.2.1. *Feature Identification*

To minimize noise and to extract the weakest coherent flux modulations, the data were binned into 11 minute intervals resulting in a total of 84 time bins. The relative changes in flux were tracked by analyzing the following variable:

$$\Delta\tau \equiv -\ln\left[\frac{F(v)}{F_{\rm avg}(v)}\right], \tag{10}$$

where $F_{\rm avg}$ is the smoothed mean spectrum plotted in Figure 1. The quantity $\Delta\tau$ is equivalent to the change in optical depth (positive or negative) required for $F_{\rm avg}$ to be attenuated to F. Because we have no a priori expectation whether the intra-DAC modulations are extra absorptions or local opacity cancellations—with respect to a steady state—normalizing by the mean flux seems like the safest method (see also, e.g., Prinja & Fullerton 1994). The identification of discrete features in the $\Delta\tau$ data was done in four general steps:

1. For each time bin, the 15 strongest minima and maxima of $\Delta\tau$ (i.e., those with the largest absolute value) in velocity space were located.

2. The velocities and strengths of these extrema were used as initial guesses in a Levenberg-Marquardt χ^2 minimization code. This algorithm fitted $\Delta\tau(v)$ to a sum of 21 Gaussian functions with parameterized central strengths,

central velocity positions, and widths. The six unspecified initial guess features were chosen at random in 10 independent trials; the trial with the lowest resulting χ^2 was kept as the best fit to the data.

3. The minima and maxima of the fitted multi-Gaussian functions were located and are plotted in Figure 3. The velocity locations of the features are denoted v_f and the extreme values of the relative optical depth are denoted $\Delta\tau_f$.

4. We took care that the features we identified were not due to other ions, especially the four Fe V lines predicted by Paper III at $\lambda\lambda$1385–1388, and we were able to identify the same patterns of features in the Si IV λ1403 component of the doublet.

Local extrema of $\Delta\tau$ were found to be more reliable as "feature locators" than the central velocities of the fitted Gaussians because many of the actual features do not resemble Gaussian functions and are automatically fitted by a sum of two or more Gaussians. The central velocities of these extra terms should not be interpreted as independent dynamical wind features. The multi-Gaussian fitting is necessary, however; it provides more robust values of v_f for the minima and maxima than can be determined from the raw (or even smoothed) data points.

As can be seen in Figure 3, the general trend is for features to accelerate from low to high blueshifted velocities. Acceleration of *coherent* structures is seen in the strongest features out to $\sim$1450 km s^{-1} and in weaker features out to $\sim$1700 km s^{-1}. (This is evidence that the terminal velocity of the wind must be significantly larger than the mean DAC velocity of 1280 km s^{-1}.) The variation of $|\Delta\tau_f|$ as a function of v_f follows closely the shape of the standard deviation curve for the Si IV flux shown in Figure 1. This is qualitatively similar to the trend observed for O-star DACs: an increase, followed by a decrease in optical depth (and column density) with increasing v_f and time (e.g., Kaper et al. 1999).

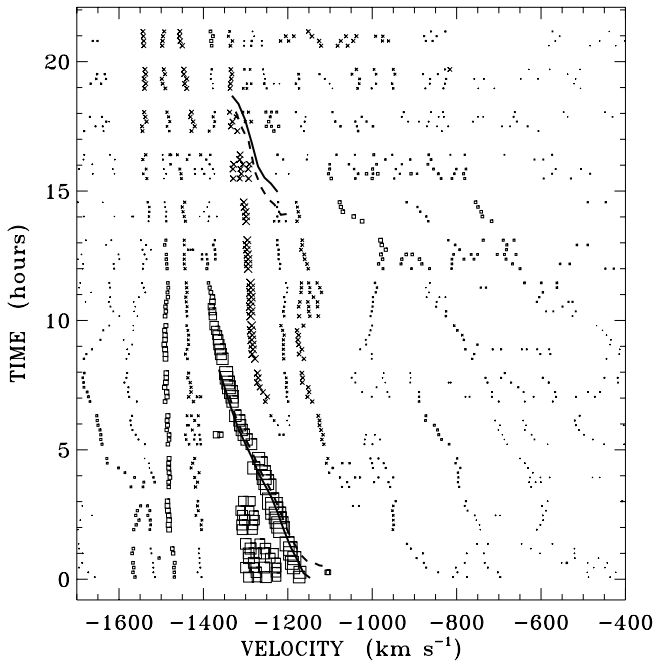

FIG. 3.—Velocity and time evolution of individual DAC features (i.e., local minima and maxima of the fitted residual flux $F/F_{\rm avg}$) for the Si IV λ1394 line. The size of each symbol is proportional to the magnitude of $\Delta\tau_f$ for that feature, with squares representing $\Delta\tau_f > 0$ and crosses representing $\Delta\tau_f < 0$ (see text). The largest symbols correspond to $|\Delta\tau_f| \approx 0.45$ and the smallest symbols correspond to $|\Delta\tau_f| \leq 0.01$. Solid and dashed lines denote time-shift correlations δt for the λ1394 and λ1403 lines, respectively (see § 3.3). Their absolute time shift is arbitrary.

3.2.2. *Acceleration of DAC Fluctuations*

The features in Figure 3 also share another characteristic of O-star DACs: they accelerate outward much more slowly than would parcels flowing with the mean stellar wind. This has led to the suggestion that DACs do not represent isolated mass-conserving "blobs," but instead they indicate the presence of a rotating pattern or perturbation through which wind material flows (e.g., Prinja et al. 1992; Prinja 1994; Cranmer & Owocki 1996). We adopt this interpretation for the features plotted in Figure 3 and refer also to the discussion in § 1 of CIRs in the solar wind. Although CIRs represent dynamical modulations in the wind's density and velocity, we believe that the bulk of the opacity fluctuations in the DACs of γ Cas arise from changes in the Si^{3+} ionization state (see § 4). The CIRs thus act as small-amplitude "seed" perturbations that are amplified by the rotationally modulated ionization variations and probably occupy the central region of a density "plateau" referred to above which gives rise to the overall DAC feature.

Figure 4 shows the computed accelerations of features identified in Figure 3; approximately 50% of the total number of features (1766) were used to compute the 132 acceleration points. Data in each of the 13 orbits of *HST* were isolated and grouped subjectively into coherent "patterns" of features that appear at similar values of v_f in at least three contiguous observations. In most cases the patterns were easy to identify, but at times the definitions may be arbitrary (one example: the 18 points between the limits $0 < t < 1.5$ hr and $-650 < v_f < -400$ km s^{-1} were grouped together as a single accelerating pattern).

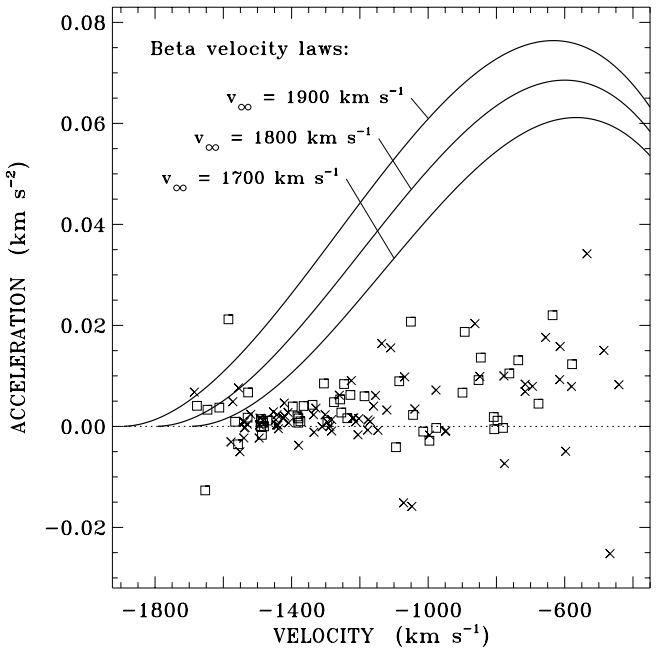

FIG. 4.—Computed accelerations of individual Si IV λ1394 DAC features (*squares*: $\Delta\tau_f > 0$; *crosses*: $\Delta\tau_f < 0$) plotted vs. v_f, and compared with the acceleration expected for parcels flowing with a $\beta = 1$ stellar wind with $v_\infty = 1700$, 1800, and 1900 km s^{-1}. Of the 132 identified features, 76% are accelerating and 24% are decelerating.

Each of the 132 patterns was fitted with a straight line in $v_f(t)$, and because the time span of each orbit does not exceed ~ 1.5 hr, higher order curvature effects are negligible. In Figure 4 the slopes (i.e., accelerations dv_f/dt) of these lines are plotted as a function of v_f. They are compared with steady state accelerations ($v_r \partial v_r/\partial r$) computed from a wind velocity law (eq. [9]) with $\beta = 1$ and three representative terminal speeds. All realistic models of time-steady hot-star winds have $\beta < 1$ and are thus more rapidly accelerating than the $\beta = 1$ case. This leads to the almost certain conclusion that the DAC features highlight dynamical perturbations that accelerate out significantly more slowly than the mean stellar wind of γ Cas. Note that 24% of the features in Figure 4 seem to *decelerate*, but we have no explanation at present for these motions.

In § 4 we interpret the features in Figures 3 and 4 as arising from varying illuminations of Si^{4+} from X-ray active centers near the star's surface, which in turn cause changes in ionization along the spiral pattern delineated by square symbols (density enhancements) and crosses (dearths of Si IV atoms, caused either by localized low-density pockets or high ionization). From the slow outward accelerations, we do not associate these symbols with discrete parcels moving outward at lower accelerations than the ambient wind but rather small-amplitude perturbations (i.e., rotating patterns akin to "streaklines") through which wind particles flow. Particles flow along primarily radial trajectories, being only slightly interrupted in their accelerating flow by the presence of the density structure. The idea of corotating patterns stems from the unlikelihood that very low-contrast blobs could form over regions of the star and flow in a far different fashion than the ambient wind. Note that the perturbations discussed in this section are superimposed upon, but independent of, the "mean DAC" density enhancement discussed in § 3.1.

3.3. *DAC Light-Curve Correlations*

We can gain further insight into the processes responsible for the 10%–20% temporal flux modulations within the DACs by examining their light curves in more detail. Figure 5 illustrates the relative flux variations at five DAC velocities and compares them with the light curve at line center. The line-center light curve is averaged over 5 pixels, or $v = \pm 30$ km s^{-1}, about the rest-frame wavelength of 1393.755 Å. As noted in Figure 4 of Paper III, the DAC variations correlate very well with the Si IV line-center flux variations, with cross-correlation coefficients up to $+0.95$ at DAC velocities of about -1270 km s^{-1}.

We also notice that the correlation between line-center and DAC light curves in Figure 5 breaks down for velocities lower and higher than -1270 km s^{-1}. However, we see that the correlation can be improved significantly by performing a *time shift* on the DAC data. For the extreme velocities plotted (-1195 and -1315 km s^{-1}), time shifts of approximately $+2$ and -2 hr, respectively, would bring the DAC and Si IV line-center light curves into better alignment and maximize their correlation coefficients. We computed time shifts δt that maximize the correlations for each blueshifted velocity in the DACs and found the function $\delta t(v)$ to be reasonably continuous and monotonic over a range of 300–500 km s^{-1} in the strongest parts of the DACs.

In Figure 3 we have overplotted $\delta t(v)$ curves at the appropriate velocities and compared them with the features identified in the previous section. Because the first and second halves of the light curves behaved slightly differently, we have plotted two sets of curves in Figure 3 for the time intervals 0–9.2 hours and 10.8–21.3 hr. Note that the absolute temporal positioning of $\delta t(v)$ is arbitrary, and the curves have been centered in their respective halves of the data to reflect the fact that they denote the centers of the patterns given by the squares. The correlation coefficients decrease at the low- and high-velocity edges of the DACs, and the curves in Figure 3 denote velocities with coefficients greater than ~ 0.95. The correlations for the Si IV λ1394 and λ1403 lines behave similarly to one another.

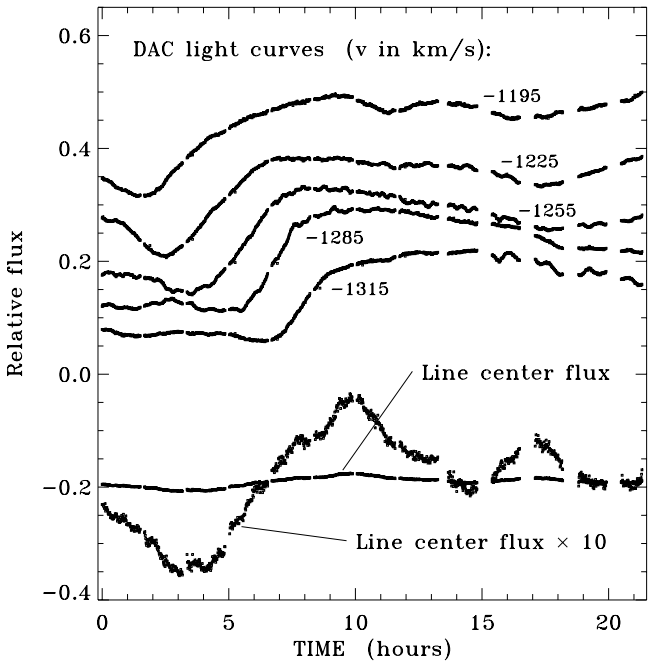

FIG. 5.—Relative flux variations of Si IV λ1394 for five blueshifted DAC velocities and for the line-center flux (the latter averaged over ± 30 km s^{-1} around $v = 0$). An expanded line-center light curve (multiplied by a factor of 10 and recentered on the original curve) is also plotted to facilitate comparison with the DAC variations.

The detailed agreement in Figure 3 between the time shift in the first half of the data and the strongest set of "absorption" features (squares with $\Delta\tau_f > 0$) between -1200 and -1400 km s^{-1} was unanticipated but is understandable. At times between 0 and 10 hr these modulations dominated the data set common to both analysis techniques. For the second half of the data, we believe that the correlation technique is more sensitive to a weak pattern embedded in the DAC than the feature identification method because the latter cannot find positive optical depths when the DAC flux level is higher than the time-averaged DAC. In particular, we suspect that the upper line in the plot is a fit to a weaker spiral density pattern emanating from a region of the star at another azimuth (perhaps 140° away from the first pattern).

4. X-RAY ILLUMINATION OF DACS AND ASSOCIATED UV LINES

We now bring together numerous strands of evidence of rapid variations of DACs in resonance lines and correlations of other UV lines from the GHRS data and archival *IUE* data for γ Cas. We point out that such correlated variability can be understood self-consistently by changes

from the radiation field of the star and indeed may not even depend sensitively on the presence of the strong mean DACs analyzed in § 3.1.

4.1. *The Illumination Scenario*

In anticipation of the further evidence presented below, we pause to discuss a powerful interpretive scenario for the various flux variations and correlations. In this scenario, corotating X-ray emitting regions on or near the star produce a variable ionization state in the circumstellar plasma. Material at different distances and longitudes is exposed to X-ray emission from only the "visible" activity centers and not those over the local horizon. This variable illumination changes the Si ionization state and produces correlated light curves at various distances. There may be different ways to explain the flux changes at Si IV line center, and in Paper III we considered and rejected a number of them. However, we believe the illumination model presented herein offers a new hypothesis which was not considered in Paper III.

As Figure 6 shows (see also § 4.2), the first minimum of the -240 km s^{-1} Si IV light curve (at about 1 hr into the time series) precedes the minimum of the line-center Si IV light curve (at 3–4 hr), as shown in Figure 5. The minimum of the line-center light curve in turn precedes the appearances of the first extrema of the UV continuum (minimum) and X-ray fluxes (maximum) at 7–8 hr. This progression of times can be understood if stationary Si IV absorbing particles at the surface do not "see" the X-ray activity centers because they are beyond the local horizon of the surface silicon atoms. In contrast, elevated material can more easily see the X-ray centers, so the silicon is more highly ionized. In order for elevated material to be shielded from these centers by its horizon, and to thus form stronger Si IV line absorptions, the elevated gas must be situated further away across the surface than the surface particles. Thus, at the time of the first minimum of Figure 6, the elevated material (arising from gas moving away from the star at about -200 km s^{-1}) is located somewhat further to the "prograde side" of the activity centers than the stationary material responsible for the Si IV zero-velocity minimum at 3–4 hr.

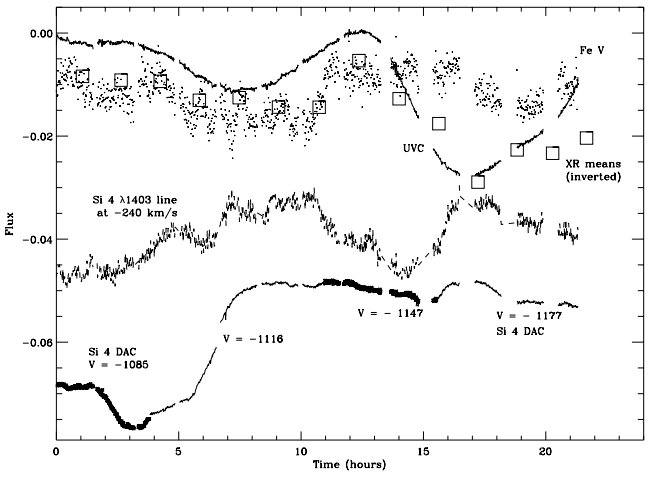

FIG. 6.—Light curves for various features of the 1996 GHRS data: UV pseudocontinuum (Paper II), multiplied by 1.5 and shifted by -1.011 (*upper solid curve*), X-ray flux variations, multiplied by -1600 (i.e., inverted) and shifted to overlay the UV continuum (*squares*), Fe V λ1413 flux (*upper dotted points*), and Si IV λ1403 flux at a blueshift of -240 km s^{-1} (*middle dashed curve*). The Si IV λ1403 DAC flux is multiplied by 0.2 and plotted for staggered blueshifts from -1085 to -1177 km s^{-1} (*lower solid curve*).

The above explanation also clarifies the existence of absorptions from slightly "cooler ion" lines of Ni II, Si III, and S IV discussed in Paper III. These lines are likewise blueshifted to about -200 km s^{-1} and show maximum absorptions at times of 3, 15, and 21 hr (see Fig. 3 of Paper III). The times of these absorption maxima coincide with the times of the blueshifted Si IV maxima. In contrast, the second and third absorption maxima in the stationary Si IV time series occur closer to the time of the occurrence of the second X-ray maximum (17 hr). So again, we see a progression of times such that the blueshifted material shows the greatest absorptions at times that are more separated from the X-ray maximum than the stationary material does. By our shielding explanation, these absorption maxima can be understood not as being due to isolated structures (two "tepid cloudlets") over certain regions of the star, but rather by the greater surface areas of the star seen by elevated, outflowing material. Such material is shielded from the X-ray flux over smaller areas of the star where it can be preferentially observed in the cooler ion lines available to us. We suspect further that the outflowing material in reality exists over much or all of the star's surface and that it represents a precursor to the wind flow visible only in some X-ray unilluminated regions over the star.

Strong evidence for changes in stellar ionizing flux causing rapid variations in the emissions of Hα and other lines has recently been given by Oudmaijer & Drew (1997) and Smith et al. (1997). This interpretation frees one of positing that a Be star must eject extremely rapidly moving symmetric shells into the circumstellar environment, but it requires that nonthermal processes occur on its surface. Since γ Cas's X-rays are likely to be emitted from sites on or near its surface (see Paper I), this requirement seems to be already met for this star.

4.2. *1996 GHRS Light Curves*

Figure 6 shows coplotted light curves of the 1996 March GHRS fluxes (1) in the UV pseudocontinuum (for definition, see Paper II), (2) at single pixels representing the Si IV λ1403 (at $v = -240$ km s^{-1}) and Fe V λ1415 lines, and (3) at a set of blueshifted velocities in the λ1403 DAC component. Also in Figure 6 are the *RXTE* orbital-averaged X-ray fluxes, inverted to emphasize the correlations referred to in Paper I and below. The fluxes in the DAC were plotted for a shifting velocity with time, from -1085 to -1177 km s^{-1}, which was required empirically to produce an optimal correlation between moderate- and high-velocity Si IV fluxes (see also Fig. 5). Note that these shifted velocities are the only ones that reproduce the sharp bump at 16–18 hr in both curves, and in fact this was a primary empirical constraint for choosing these velocities.

Figure 6 shows a general direct correlation between the inverted X-ray fluxes, the UV continuum, and Fe V *absorption* line fluxes. Likewise, the fluxes of the moderate-velocity Si IV absorption are anticorrelated with the UV continuum and high-energy variations. In addition to these correlations, Smith (2000) showed that the fluxes of the Si III absorption line—which appears at a moderate blueshift—are well correlated with the fluxes of the Si IV line in this data set. These line flux correlations suggest ionization changes in the absorbing medium (density variations being effectively ruled out by the Fe V data). Their respective

correlations or anticorrelations suggest further that the X-ray flux is the driving factor. We tie this association to DAC variations in the discussion below.

In Paper III it was found that in order to reproduce the strengths of sharp, high-velocity Fe V and Si IV features in the spectrum of γ Cas, a plasma temperature is required that is higher than that predicted by radiative equilibrium models. Indeed, the Fe V opacity is highest for radiative temperatures of 35,000 K or higher, given reasonable densities (10^{11}–10^{12} cm^{-3}). At this temperature, silicon is substantially ionized to Si^{4+}. Thus, these correlations can be explained by brief changes in ionization in the circumstellar plasma, with Fe V line strengthenings and Si III/Si IV weakenings being associated with increases in ionization, probably from illumination by greater than average X-ray fluxes. This supports the preliminary interpretation of the DAC flux variations given in § 4.1. Note that the staggered DAC light curve in Figure 6 is relatively flat at times of 8–14 hr when compared with the other (lower velocity) light curves, thereby lowering the quality of the correlations. At this rotational phase, we believe that features far from the star see two or more X-ray emitting regions on opposite limbs of the star which can mute the strong rotational modulation felt by parcels closer to the star (see also § 5).

4.3. *1982 Archival IUE Data*

In 1982 January, a monitoring campaign was conducted on γ Cas with the *IUE* satellite. Thirty-two high-dispersion exposures were obtained through the small aperture of the Short Wavelength Prime Camera continuously over 44 hr. We obtained the NEWSIPS-processed MXHI files from NASA/STScI's Multi-Mission Archive at Space Telescope (MAST) facility, co-added them, and obtained difference spectra in the echelle orders containing the C IV and Si IV lines. We discovered that the flux at high blueshifted velocities in the C IV and, to a lesser extent, Si IV lines showed brief absorption enhancements at various intervals during this time series. In 1982 the time-averaged DAC was considerably weaker than in 1996, yet in both epochs the DACs of Si IV or C IV showed rapid variations. Figure 7 shows nine strengthenings that could be identified in the C IV $\lambda\lambda$1548, 1551 difference spectra, in each case centered at

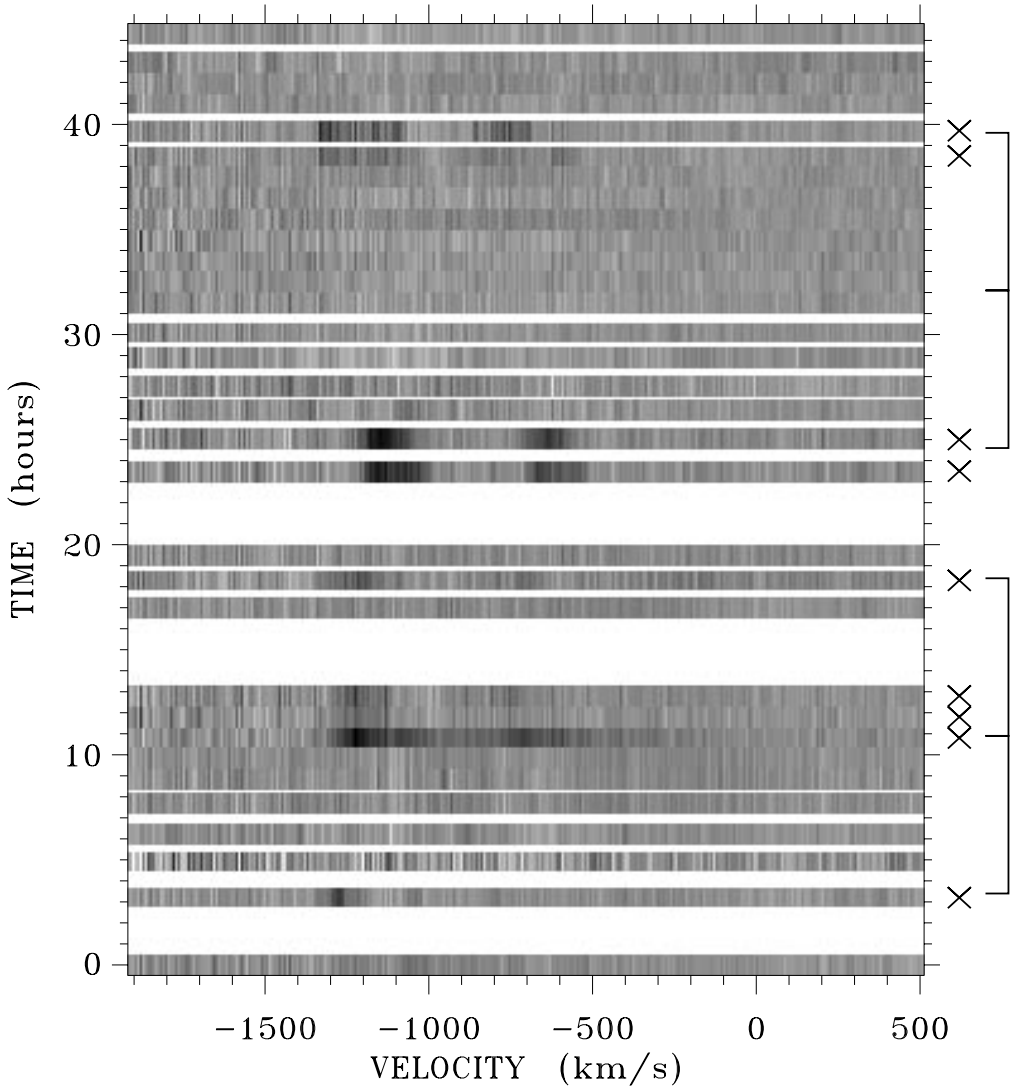

FIG. 7.—Gray-scale dynamic difference spectrum of C IV $\lambda\lambda$1548, 1551, plotted vs. the Doppler velocity of the blue (λ1548) component and time from the start of the observation. The plotted quantity is the *IUE* flux minus the time-averaged spectrum, and horizontal white bars represent periods of no data. Strong DAC absorption enhancements are denoted on the right by crosses, and the vertical combs show the 7.5 hr X-ray flare periodicity.

velocities of -1100 to -1300 km s^{-1}. The strongest difference feature was 18% of the time-averaged flux, which is approximately the same magnitude of the variability (10%–20%) in the 1996 March GHRS observations. We were similarly able to find weaker enhancements (up to 6%) in *IUE* data we obtained to support the GHRS observations in 1996 January.

In Figure 8 we show the ultraviolet continuum (UVC) light curve at two wavelengths in the 1982 data set, along with cross symbols denoting times of the strongest DAC differences in Figure 7. The UVC curves show the same "dips" we reported in Papers I and II from the 1996 data and which can be phased together with that data set to obtain a period of 1.123 days or a close alias thereof (Robinson & Smith 2000). Inspection shows the DAC strengthenings are associated with the UVC dips. Moreover, the amplitudes of these two features are roughly correlated, showing smaller amplitudes for each of the three dips at 8–17, 22–27, and 38–43 hr. Robinson & Smith (2000) have pointed out that they are likely to be variable from cycle to cycle, an inference supported by different X-ray flux extrema from one cycle to the next in *RXTE* data from 1998 November. Thus, we have new evidence from the 1982 *IUE* data that illuminations of DAC material are modulated from cycle to cycle.

The appearance of DAC strengthenings may also have a periodic component. Robinson & Smith (2000) found a robust cross-correlation in the inverse X-ray fluxes from γ Cas in both their 1996 March and 1998 November data sets. In particular, they found that the X-ray flares from this star tend to "turn off" with fair regularity every $\sim$7.5 hr, even during the times of maximum flaring that coincide more or less with the passage of the UVC bumps (see also Paper I). According to the previous section, if the illumination hypothesis is valid, the DAC strengthenings must actually correspond to *decreases* of the exciting X-ray flux. In Figures 7 and 8 we denote by comb symbols the times of successful recurrences of the DAC strengthenings with the $\sim$7.5 hr cyclicity (separate combs are shown because one interval is 6.2 hr). The only significant "miss" is at a time of 31 hr, which is equidistant between the two UVC dips. This corresponds to the passage of a region on the star's surface that is comparatively devoid of active X-ray centers and hence fluctuations.

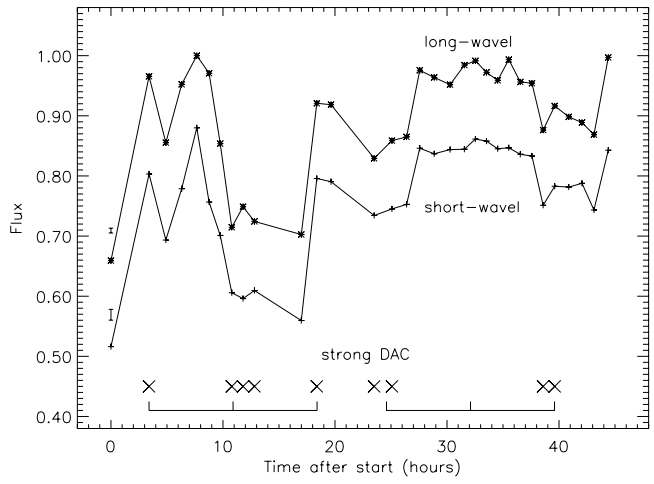

FIG. 8.—*IUE* ultraviolet continuum variations at two sets of wavelengths: 1775–1875 Å (*upper curve*) and 1210–1260 Å (*lower curve*). Statistical uncertainty limits of $\pm 1\ \sigma$ are denoted by error bars on the left. The DAC absorption enhancements and X-ray flare periodicities are plotted with crosses as in Fig. 7.

It is worth pointing out that in their comprehensive study of DAC variability in γ Cas, Telting & Kaper (1994) did not notice the rapid flickering. Indeed, even now such DAC behavior has not been noticed for other Be stars. Since their sample included an average of only every fourth spectrum, they could not have detected variability on a time scale of $\leq$2 hr. Nonetheless, in Figures 8–10 of their paper it is interesting to compare the amplitude of their scatter in derived optical depths in the DACs observed the 1982.0 series as compared to the increases in optical depths during 1987–1988, at a time when the precessing, one-armed disk density enhancement produced strong DACs (see § 5). The increases in the 1987–1988 epoch should be considered a measure of the effect of increased density in the N V, C IV, and Si IV lines. The Telting & Kaper data show that the N V DACs have a proportionately smaller range in optical depth than the DACs of C IV or Si IV. Since the DAC strengthenings occur in the same velocity range and therefore in the same volume of the wind, the changes in optical depths are more likely to be due to differing ionizations than densities. This emphasizes that the rapid variations in DAC features probably result from changes in ionizing flux from the star.

4.4. *Supporting Evidence from Copernicus Studies*

Previous studies on γ Cas with *Copernicus* by Slettebak & Snow (1978) and Marlborough, Snow, & Slettebak (1978) showed changes in several UV lines on timescales of minutes to hours that make sense only in the context of ionization enhancements caused by rapid variations of X-ray flux. The first of these papers reports the observations of a surge in Hα emission on the night of 1977 January 29. At this same time the *Copernicus* spectrometer, which took several minutes in a spectral scanning mode to move from one line to another, observed a weak emission bump in the Si IV λ1394 line but not in its doublet component at λ1403 several minutes later. A similar anomaly was noticed about an hour later: the Mg II λ2795 line showed strong emission, while λ2802 exhibited almost none.

There is even more to this interesting report. The *Copernicus* satellite consisted of co-aligned UV and X-ray telescopes, and unbeknownst to Slettebak & Snow (1978), the *Copernicus* X-ray telescope observed an increase in X-ray flux at this same time—a fact reported by Peters (1982), R. S. Polidan (1999, private communication), and A. N. Parmar (1999, private communication). These data were never published, so one cannot prove what actually happened at this time. Nonetheless, the combined claim of these optical/UV/X-ray correlations has credence if one accepts that the Si IV line responds to large fluctuations in X-ray emissions. These fluctuations can take the form of either (1) a decrease in the mean emission rate (resulting in increased absorptions; see Robinson & Smith 2000), or (2) the occurrence of several flares at the same time (decreased Si IV line absorption), as occurs occasionally (Murakami et al. 1986; Paper I).[6] In a similar vein, the report by Marlborough et al. (1978) of a decrease in the DAC absorption

[6] The emissions of Hα and Mg II occur over large volumes and hence at great distances from the star. Thus, changes in their strengths are difficult to explain in any other way than by illumination from the star.

strength in 3 hr may also be understood by a surge in X-ray flares over this period.

5. DISCUSSION

In this paper we have found strong evidence for the existence of corotating streams of varying ionization in the supersonic wind of γ Cas. In addition, the strong blueshifted DACs in the 1996 GHRS data probably signify the presence of a broad plateau of high density, disk-enhanced material in the wind. These two phenomena contribute to an already complex circumstellar environment (see also Papers I, II, and III). They also seem consistent with the general scenario of active magnetic fields above the photosphere of γ Cas.

The first major result of this paper is the determination of the density in the time-averaged DAC (§ 3.1), which is at least an order of magnitude larger than the mean polar wind. Doazan et al. (1987) and Telting & Kaper (1994) found that DACs occur more frequently and with larger opacity when the Balmer emission lines exhibit a stronger violet than red peak ($V > R$). As discussed in § 1, the prevailing interpretation for the cyclical, several-year period V/R variations is the prograde precession of a one-armed ($m = 1$) density oscillation (see also Savonije & Heemskerk 1993; Telting et al. 1994; Hanuschik et al. 1995; Savonije 1998). When the high-density part of the oscillation resides on the approaching side of the disk, Doppler blueshifts will result in $V > R$, and angular momentum conservation will carry wind parcels in the direction of rotation (in the inertial frame) as they accelerate. These dense parcels may eventually occult the star and thus create strong absorption features in the wind (see Fig. 12 of Telting & Kaper 1994).

The puzzle in the above scenario is how the presumably nonexpanding (or subsonically expanding) Keplerian disk interacts with the supersonic polar and midlatitude wind to create the observed DACs. Recall that interferometric and polarimetric data have constrained the inclination angle i of γ Cas to be approximately 45°, so dense material from a thin equatorial disk would have to migrate to a relatively high latitude in order to occult the star. We envision two broad classes of dynamical wind-disk interaction:

1. *Shear and entrainment.*—If the $m = 1$ disk perturbations are even partially adiabatic, an increase in the density should result in an increase in temperature. This increases the vertical scale height of the disk, allowing higher density gas to reach higher latitudes. The strong shear between the supersonic wind and the "puffed-up" disk material can give rise to a number of complex hydrodynamical phenomena: entrainment at grazing incidence, turbulent mixing, Rayleigh-Taylor instability, shock compression, and reaccretion onto the star (e.g., Elmegreen 1978, 1979; Raga, Cabrit, & Cantó 1995; Bjorkman & Wood 1995).

2. *Disk winds.*—Keplerian accretion and decretion disks in various types of stellar environments have been shown to be able to drive substantial winds from their surfaces (see recent work by Woods et al. 1996; Pereyra, Kallman, & Blondin 1997; Proga, Stone, & Drew 1998). Such vertical flows may be enhanced by the presence of a higher density one-armed perturbation in the inner regions of the disk. Most postulated varieties of disk wind in early-type systems are driven by the same line radiative forces that drive the mean polar and midlatitude stellar winds. However, for disks, there are numerous issues concerning the nonisotropic nature of the scattering opacity that gives rise to radiative forces, and current models are only beginning to explore the possible solution regimes (e.g., Gayley, Owocki, & Cranmer 1999).

No matter which effects dominate the midlatitude disk-enhanced wind of γ Cas, the presence of added density in the wind where the DACs are formed must have some dynamical feedback (e.g., Owocki 1998). The wind's line-driving forces are inversely proportional to density (see Castor, Abbott, & Klein 1975), so a disk-enhanced stellar wind may not be accelerated as rapidly as its undisturbed portions. Also, if the wind density grows high enough, parcels of gas may not be drivable to infinity and thus could "stall" and reaccrete, possibly cyclically (Porter & Skouza 1999). Finally, magnetic interactions between a supersonic wind and a Keplerian disk are nontrivial, and Paper III described some of the dynamical consequences of possible star-disk interactions.

The second major result of this paper is the uncovering of multiple lines of evidence for X-ray illuminated regions of modulated Si IV ionization in the wind (§§ 3.2–3.3, § 4). The ultraviolet continuum and the inverted X-ray flux have been shown to anticorrelate generally with the Si IV flux variations (Fig. 6). Our interpretation is that an increased X-ray flux results in a higher Si ionization state (Si V is the dominant stage in the DAC material of γ Cas), a reduced Si IV fraction, and thus a decreased line absorption and a higher flux. The line-center ($v = 0$) Si IV flux variations are reflected nearly simultaneously in the blueshifted DACs, which represent wind regions that experience the same absence of a source of ionizing radiation, and even the 7.5 hr cessations in X-ray flaring (Fig. 8). The staggered, time-shifted DAC light curves in Figures 5 and 6 reveal the shapes of these corotating regions in the accelerating wind. In our interpretation, if γ Cas had no near-surface X-ray activity centers, the DAC features would have a more uniform (though possibly greater) strength over the entire time series, with any corotating spiral features being equally visible at all times.

Figure 9 shows a schematic illustration of the circumstellar environment of γ Cas as revealed by the GHRS and *RXTE* data. The kinematic DAC features identified in § 3.2 are plotted as in Figure 3, but only the features used to compute the acceleration points in Figure 4 are displayed. Time is translated into azimuthal angle assuming a rotation period of 1.12277 days (Robinson & Smith 2000), and velocity is translated into radial distance using equation (9) with $\beta = 1.9$. *The latter transformation is merely illustrative and is not meant to imply acceleration of individual parcels to individual distances.* The two strongest circumstellar clouds identified in Paper II are plotted using the "reference latitude" parameters in Table 1 of Paper II. Also, 1 minute averaged X-ray fluxes are plotted in the outermost ring of Figure 9, and there is a clear anticorrelation between the X-ray flux level and the overall strength of the DAC fluctuations.

Also indicated in Figure 9 are continuous spirals fitted through several prominent flux variations in the DACs. In evaluating this figure, the reader can rotate the page to simulate the attributes of the cloud and Si IV signatures at different times, remembering that the various spiral patterns are thought to corotate with the star. We interpret the

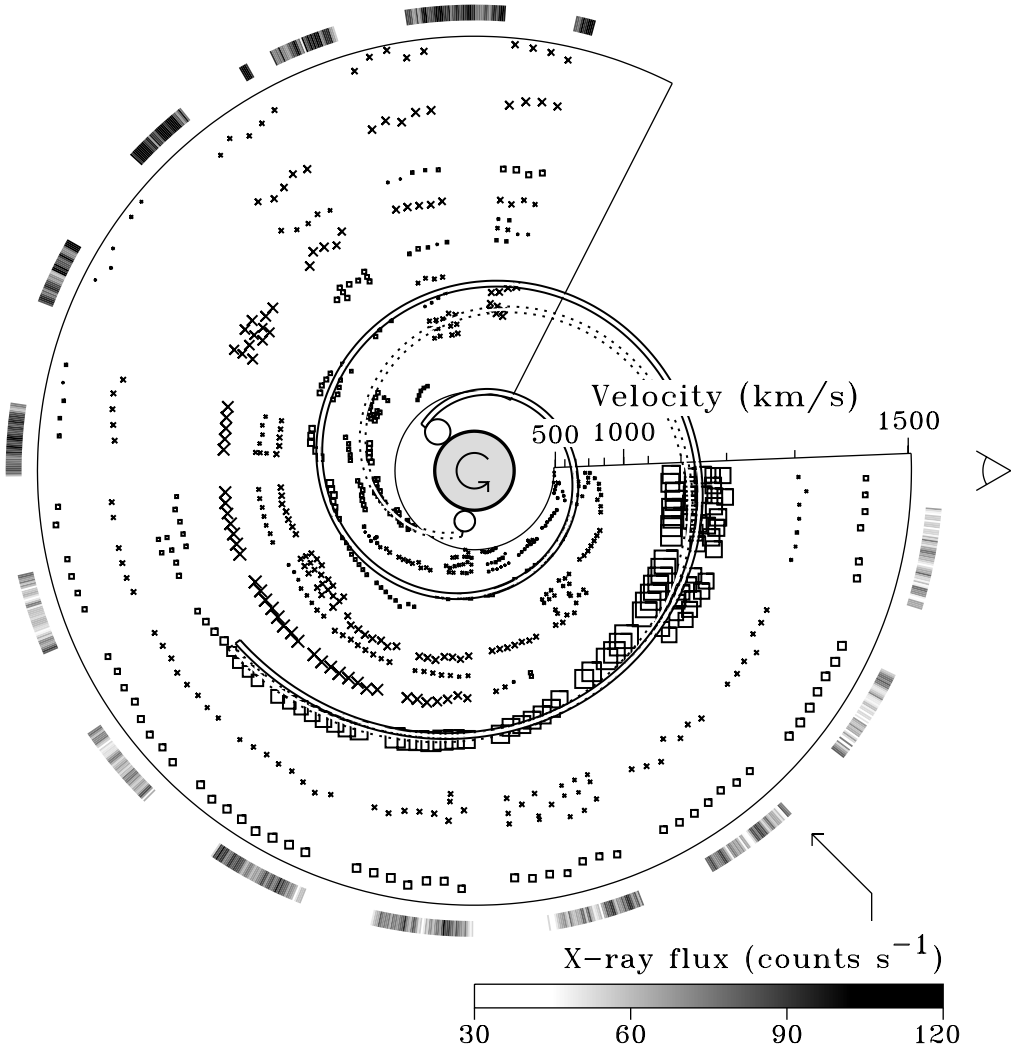

FIG. 9.—Schematic illustration of γ Cas with the two strongest circumstellar clouds from Paper II depicted as circles on the star's surface. The DAC flux variations shown are identified in Fig. 3 (*squares* and *crosses*), and *RXTE* X-ray flux variations (*gray scale in outer ring*) are taken from Paper I. The DAC features actually lie in a "cone" at an inclination angle of $i \approx 45°$, which is flattened out here. Velocity is mapped into distance using an ad hoc $\beta = 1.9$ velocity law and is only suggestive of actual radial structure. The spiral features originating at the clouds have the following parameterizations: $r/R_* = 0.001(11.4 + \psi)^{2.71}$ (*solid spiral*), $r/R_* = 0.589(0.580 + \psi)^{1.14}$ (*dotted spiral*), where ψ is an azimuthal "streakline" angle measured clockwise in radians from the positive x-axis (*eye symbol on right*).

squares and crosses in Figure 9 as arising from varying illuminations of Si^{4+} (and thus changes in Si^{3+} in the opposite sense) from X-ray active centers near the star's surface, which vary due to the star's rotation and because of more rapid fluctuations in the flaring level. We remind the reader that the DAC is optically thin to $\lambda 275$ radiation, so material in the inner DAC does not shield silicon atoms from illumination effects. It should also be pointed out that a correlation between X-ray flux and DAC weakness should not be instantaneous because of the finite recombination time scale of DAC material. According to the DAC densities given in Figure 2, this timescale should be of order several minutes to a few hours. Thus, this picture predicts that in general it is more likely that DAC features will decay abruptly (i.e., with the sudden appearance of a flare) than appear (owing to recombination of Si^{4+}).

There is insufficient observational evidence to be able to determine exactly the azimuthal origin of the DAC variations, so the precise spirals plotted in Figure 9 are our conjectures. Note, however, that in Paper II the "primary" cloud at phase ~ 0.6 (Fig. 9, *upper left*) was constrained to exist at a higher range of latitudes (30°–60°) than the "secondary" cloud (15°–30°). If the X-ray illumination variations persist in latitude into the wind, there seems to be a better chance that the primary cloud gives rise to observable ($i \approx 45°$) DAC variability. The tight "winding" plotted in Figure 9 for this feature was suggested by recalling the low-velocity (-200 to -500 km s^{-1}) accelerations in the Si IV GHRS data (see Fig. 1 of Paper III).

A few comments concerning Figure 9 are in order. First, the narrowness of the spirals is to some extent an artifact of using the minima and maxima in the fitted $\Delta\tau$ (§ 3.2). Second, the primary spiral occurs where the DAC is optically thick, so fluctuations may actually represent the highlighting of density perturbations over an appreciable radial distance. Third, despite the still substantial X-ray fluctuations late in the observations, there are fewer DAC fluctuation symbols in the figure at these times, particularly in the -1200 to -1300 km s^{-1} range. This is because the high X-ray fluxes force silicon to be even more in the form of

Si^{4+}, so there are fewer Si^{3+} atoms to effect a change in the DAC. Moreover, the DAC is optically thick in this velocity range, so small variations may be muted.

A fourth comment concerning Figure 9 is that the absorption features at phase 0 (Fig. 9, *right-hand side*) and -1470 km s^{-1} may represent the next winding of the highest opacity spiral below it at -1200 to -1300 km s^{-1}. However, the spiral "fit" curves accelerate too rapidly to pass through these features: they just exceed -1500 km s^{-1} slightly before the data resume at phase 0. This suggests that the spiral structures eventually become more tightly wound than could be explained by such a simple parameterization. Fifth, note the interesting fading of the spiral pattern shown by the squares in Figure 9 at -1300 km s^{-1} and at phase ~ 0.4. This fading occurs at the same time two low-velocity ($\gtrsim -1000$ km s^{-1}) spiral-absorption patterns are present. This fits into our illumination context if the "inner" spiral material cannot see the X-ray centers associated with both clouds (hence the material becomes visible to us as features in the lesser excited ion stage of Si^{3+}) whereas the clouds are visible well within the horizon limits of the stellar disk as seen by material in the outer spiral, which is therefore ionized to Si^{4+}. Similarly, as one starts out along the primary spiral in Figure 9, the abrupt decrease in the DAC enhancements at about 200 minutes can be understood qualitatively in this scheme as matter responding to increased illumination as the X-ray activity centers associated with the secondary cloud (at the bottom of the stellar disk in Fig. 9) become visible at the horizon.

As suggested above, the corotating wind modulations that give rise to DAC variability may originate with the circumstellar clouds of γ Cas. The observed properties of these clouds (Paper II) are consistent with what is expected for magnetic prominences, and the presence of such features has been inferred around late- and early-type magnetic variables such as AB Dor and σ Ori E (Collier Cameron & Robinson 1989; Bolton 1994). Matter at the tops of closed-field magnetic loops is subject to an unstable force balance (e.g., Wang et al. 1998), and the wind that emerges from these regions should interact with the wind from open-field regions to produce CIR-like azimuthal structures (Mullan 1984, 1986; Cranmer & Owocki 1996). In the wind of γ Cas, the CIRs may be shocks or gradient discontinuities that arise because of wind inhomogeneities emanating from very near the surface of the star.

Because the winds of Be stars are normally too tenuous to produce strong P Cygni line features, CIR structures may or may not be visible as they rotate in front of the star. As we have seen, though, two effects help to increase the magnitude of the resulting opacity modulations for γ Cas: (1) decreases in the silicon-ionizing flux and (2) the presence of the increased density in the wind owing to the mean DAC. The precise dynamical relationship between the illumination variations and the resulting blueshifted flux changes is nontrivial. One final example of this complexity is the fact that the "staggered" DAC light curve in Figure 6 (which is required to produce the best correlation with the low-velocity Si IV light curve) has velocities 100–200 km s^{-1} slower than the primary DAC absorption features in Figures 3 and 9. The staggered velocities of -1100 to -1200 km s^{-1} correspond to broad quasi-emission features (*crosses*) in these figures. We suspect that the correlation-velocity shift is the result of the large, diluted interspiral region that dominates the Si IV signal at large blueshift. Note also that the correlations between various line fluxes in the GHRS data (e.g., Si IV and Fe V) are not exact because the ionization variations probably occur in different volumes within the overall corotating material.

The 1982 *IUE* data examined in § 4.3 showed DAC modulations that were correlated with decreases in the illuminating X-ray flux, consistent with the above scenario, but at an epoch where time-averaged DACs were significantly weaker (note also that $V \lesssim R$ at that time). The rotational modulation of X-ray centers and wind ionization variations thus seem to be *independent* of the state of the time-averaged DACs and the V/R phase of the equatorial disk. In other words, depending upon the precession phase of the one-armed structure in the disk, an observer is always looking through a greater or lesser amount of DAC material to γ Cas over a rotation cycle. In 1996, the wind streams are both illuminated by the star and density-enhanced by the disk's one-armed perturbation, but in 1982 only the illuminations make the streams visible in the UV lines for brief intervals. The rotation of a CIR spiral (with varying silicon ionization) across the occulting volume in front of the star does seem to be the best explanation for the slowly accelerating DAC flux modulations at both epochs.

6. CONCLUSIONS

There are several fundamental results that have emerged from this study of the ultraviolet and X-ray variations of γ Cas. The strong blueshifted DACs in 1996 highlight the presence of a strong local maximum in the wind density along the line of sight. This feature seems to be causally connected to the equatorial one-armed density enhancement on the approaching limb of the circumstellar disk.[7] Embedded within this "disk-enhanced" wind density enhancement are lower contrast spiral-shaped variations in wind density or velocity that seem to emanate from corotating regions nearer to the surface of γ Cas. These wind streams accelerate too slowly to be propagating along with the mean stellar wind and instead seem to be corotating structures through which the wind flows. A varying illumination from X-ray centers on the star alters the Si IV ionization fraction along the line of sight, and this produces correlated variability in the DAC light curves. This variability exists in epochs of both strong and weak time-averaged DACs, which indicates that the illumination variations are not related to the precession of large-scale density modulations in the circumstellar disk. We expect further from changes in the X-ray flux patterns from cycle to cycle (Robinson & Smith 2000) that many of the detailed features in the DAC fluctuations and time histories of lines other than Si IV might never repeat exactly the same way from cycle to cycle.

This work, together with Papers I, II, and III, has provided a large number of empirical constraints on possible theoretical models of the circumstellar environment of γ Cas. It is by now well known (Massa et al. 1995a; Kaper et al. 1999) that the winds of many O and B stars exhibit rotationally modulated variations. In this work we have shown that the modulations of the wind density at a given distance from

[7] We note that the "migrating subfeatures" discussed in Paper III and the one-armed disk mapped by Berio et al. (1999) were both placed by these authors at $\sim 1.5\ R_*$ above the star's surface. The density plateau causing the DAC also probably overlaps this distance at some azimuths, so we would *expect* interactions from structures that come close together every rotation cycle.

the star are actually small ($\lesssim 25\%$) and that the majority of the time variability in our data is consistent with changes in illumination from X-ray centers on or close to the surface of the star.

For Be stars in general, it also remains to assess the relative contribution of nonradial pulsations to the stellar and wind variability (see, e.g., Baade & Balona 1994). The constructive interference of multiple oscillations has been suggested as causes of both early-type stellar wind modulations (Gies et al. 1999) and Be-star mass outbursts (e.g., Rivinius et al. 1998). Be stars such as γ Cas form a new class of early-type X-ray stars for which circumstellar magnetic fields are dynamically important (see also Underhill & Fahey 1984). In addition, a magnetic dynamo (Airapetian 2000) may play a crucial role in the evolution of Be stars and in the relationships between rapid rotation, pulsation, enhanced mass loss, and thus the Be phenomenon (see also Fabregat & Torrejón 1999).

This paper is dedicated to the memory of Professor Arne Slettebak. The authors would like to thank Stan Owocki and Lex Kaper for many valuable discussions and Damian Christian for help in calculating EUV opacities. The access of the *IUE* data was made possible by the National Space Science Data Center (NSSDC/NDADS) at Goddard and the Multi-Mission Archive at Space Telescope (MAST). This work is supported by the National Aeronautics and Space Administration under contract GO-6086.01-94A, and by grant NAG5-7822 to the Smithsonian Astrophysical Observatory.

REFERENCES

Abbott, D. C., & Lucy, L. B. 1985, ApJ, 288, 679
Airapetian, V. S. 2000, in ASP Conf. Ser., The Be Phenomenon in Early-Type Stars, ed. M. Smith, H. Henrichs, & J. Fabregat (San Francisco: ASP), in press
Baade, D., & Balona, L. A. 1994, in IAU Symp. 162, Pulsation, Rotation and Mass Loss in Early-Type Stars, ed. L. Balona, H. Henrichs, & J. Le Contel (Dordrecht: Kluwer), 311
Balona, L. 1999, MNRAS, 306, 407
Balona, L., & Kaye, A. B. 1999, ApJ, 521, 407
Berio, P., Stee, P., Vakili, F., Mourard, D., Bonneau, D., Chesneau, O., Thureau, N., Le Mignant, D., & Hirata, R. 1999, A&A, 345, 203
Bjorkman, J. E., & Wood, K. 1995, BAAS, 27, 841
Böhm, T., et al. 1996, A&AS, 120, 431
Bolton, C. T. 1994, Ap&SS, 221, 95
Burlaga, L. F. 1984, Space Sci. Rev., 39, 255
Castor, J. I., Abbott, D. C., & Klein, R. I. 1975, ApJ, 195, 157
Collier Cameron, A., & Robinson, R. D. 1989, MNRAS, 236, 57
Cranmer, S. R., & Owocki, S. P. 1996, ApJ, 462, 469
Doazan, V. 1982, in B Stars with and without Emission Lines, ed. A. Underhill & V. Doazan (NASA SP-456) (Washington, DC: NASA), 277
Doazan, V., Rusconi, L., Sedmak, G., Thomas, R. N., & Bourdonneau, B. 1987, A&A, 182, L25
Elmegreen, B. G. 1978, Moon Planets, 19, 261
———. 1979, A&A, 80, 77
Fabregat, J., & Torrejón, J. M. 1999, A&A, 357, 451
Feldmeier, A., Puls, J., & Pauldrach, A. W. A. 1997, A&A, 322, 878
Fullerton, A. W., Massa, D. L., Prinja, R. K., Owocki, S. P., & Cranmer, S. R. 1997, A&A, 327, 699
Gayley, K. G., Owocki, S. P., & Cranmer, S. R. 1999, ApJ, 513, 442
Gies, D. R., et al. 1999, ApJ, 525, 420
Grady, C. A., Bjorkman, K. S., & Snow, T. P. 1987, ApJ, 320, 376
Grevesse, N., & Sauval, A. J. 1998, Space Sci. Rev., 85, 161
Hanuschik, R. W., Hummel, W., Dietle, O., & Sutorius, E. 1995, A&A, 300, 163
Henrichs, H. F., Hammerschlag-Hensberge, G., Howarth, I. D., & Barr, P. 1983, ApJ, 268, 807
Henrichs, H. F., Kaper, L., & Zwarthoed, G. A. A. 1988, in A Decade of UV Astronomy with *IUE* (ESA SP-281) (Paris: ESA), 2, 145
Horaguchi, T., et al. 1994, PASJ, 46, 9
Howarth, I. D., & Prinja, R. K. 1989, ApJS, 69, 527
Hummel, W., & Hanuschik, R. W. 1997, A&A, 320, 852
Hundhausen, A. J. 1972, Coronal Expansion and Solar Wind (Berlin: Springer)
Kaper, L., Henrichs, H. F., Nichols, J. S., Snoek, L. C., Volten, H., & Zwarthoed, G. A. A. 1996, A&AS, 116, 257
Kaper, L., Henrichs, H. F., Nichols, J. S., & Telting, J. H. 1999, A&A, 344, 231
Lamers, H. J. G. L. M., & Waters, L. B. F. M. 1987, A&A, 182, 80
Marlborough, J. M., Snow, T. P., Jr., & Slettebak, A. 1978, ApJ, 224, 157
Mason, K. O., White, N. E., & Sanford, P. W. 1976, Nature, 260, 690
Massa, D., et al. 1995a, ApJ, 452, L53
Massa, D., Prinja, R. K., & Fullerton, A. W. 1995b, ApJ, 452, 842
Mihalas, D. 1978, Stellar Atmospheres (2d ed.; San Francisco: W. H. Freeman)
Millar, C. E., & Marlborough, J. M. 1999, ApJ, 516, 276
Mourard, D., Bosc, I., Labeyrie, A., Koechlin, L., & Saha, S. 1989, Nature, 342, 520
Mullan, D. J. 1984, ApJ, 283, 303
———. 1986, A&A, 165, 157
Murakami, T., Koyama, K., Inoue, H., & Agrawal, P. C. 1986, ApJ, 310, L31
Okazaki, A. T. 1991, PASJ, 43, 75
Okazaki, A. T. 1997, A&A, 318, 548
Oudmaijer, R. D., & Drew, J. E. 1997, A&A, 318, 198
Owocki, S. P. 1998, in Variable & Nonspherical Stellar Winds in Luminous Hot Stars, ed. B. Wolf, O. Stahl, & A. Fullerton (Berlin: Springer), 294
Owocki, S. P., Castor, J. I., & Rybicki, G. B. 1988, ApJ, 335, 914
Papaloizou, J. C., Savonije, G. J., & Henrichs, H. F. 1992, A&A, 265, L45
Pauldrach, A. W. A., Puls, J., & Kudritzki, R.-P. 1986, A&A, 164, 86
Pereyra, N. A., Kallman, T. R., & Blondin, J. M. 1997, ApJ, 477, 368
Peters, G. J. 1982, PASP, 94, 157
———. 1998, in Variable & Nonspherical Stellar Winds in Luminous Hot Stars, ed. B. Wolf, O. Stahl, & A. Fullerton (Berlin: Springer), 32
Porter, J. M., & Skouza, A. 1999, A&A, 344, 205
Prinja, R. K. 1988, MNRAS, 231, 21P
———. 1994, in IAU Symp. 162, Pulsation, Rotation, and Mass Loss in Early-Type Stars, ed. L. Balona, H. Henrichs, & J. Le Contel (Dordrecht: Kluwer), 507
Prinja, R. K., et al. 1992, ApJ, 390, 266
Prinja, R. K., & Fullerton, A. W. 1994, ApJ, 426, 345
Prinja, R. K., & Howarth, I. D. 1984, A&A, 133, 110
Proga, D., Stone, J. M., & Drew, J. E. 1998, MNRAS, 295, 595
Quirrenbach, A., et al. 1997, ApJ, 479, 477
Raga, A. C., Cabrit, S., & Cantó, J. 1995, MNRAS, 273, 422
Rivinius, T., Baade, D., Štefl, S., Stahl, O., Wolf, B., & Kaufer, A. 1998, A&A, 333, 125
Robinson, R. D., & Smith, M. A. 2000, ApJ, submitted
Savonije, G. J. 1998, in Cyclical Variability in Stellar Winds, ed. L. Kaper & A. Fullerton (Berlin: Springer), 337
Savonije, G. J., & Heemskerk, M. H. M. 1993, A&A, 276, 409
Secchi, A. 1867, Astron. Nachr., 68, no. 1612, 63
Shore, S. N., & Brown, D. N. 1990, ApJ, 365, 665
Short, C. I., & Bolton, C. T. 1994, in IAU Symp. 162, Pulsation, Rotation, and Mass Loss in Early-Type Stars, ed. L. Balona, H. Henrichs, & J. Le Contel (Dordrecht: Kluwer), 171
Slettebak, A., & Snow, T. P., Jr. 1978, ApJ, 224, L127
Smith, M. A. 1995, ApJ, 442, 812
———. 2000, in ASP Conf Ser., The Be Phenomenon in Early-Type Stars, ed. M. Smith, H. Henrichs, & J. Fabregat (San Francisco: ASP), in press
Smith, M. A., Murakami, T., Ezuka, H., Anandarao, B. G., Chakraborty, A., Corcoran, M. F., & Hirata, R. 1997, ApJ, 481, 479
Smith, M. A., Robinson, R. D., & Corbet, R. H. D. 1998a, ApJ, 503, 877 (Paper I)
Smith, M. A., Robinson, R. D., & Hatzes, A. P. 1998b, ApJ, 507, 945 (Paper II)
Smith, M. A., & Robinson, R. D. 1999, ApJ, 517, 866 (Paper III)
Sparks, W. M., & Fischel, D. 1971, Partition Functions and Equations of State in Plasmas (NASA SP-3066) (Washington, DC: NASA)
Stee, P., de Araújo, F. X., Vakili, F., Mourard, D., Arnold, L., Bonneau, D., Morand, F., & Tallon-Bosc, I. 1995, A&A, 300, 219
Štefl, S., Baade, D., Rivinius, T., Stahl, O., Wolf, B., & Kaufer, A. 1998, in ASP Conf. Ser. 135, A Half Century of Stellar Pulsation Interpretation, ed. P. Bradley & J. Guzik (San Francisco: ASP), 348
Struve, O. 1931, ApJ, 73, 94
Taylor, A. R., Dougherty, S. M., Waters, L. B. F. M., & Bjorkman, K. S. 1990, A&A, 231, 453
Telting, J. H., Heemskerk, M. H. M., Henrichs, H. F., & Savonije, G. J. 1994, A&A, 288, 558
Telting, J. H., & Kaper, L. 1994, A&A, 284, 515
Underhill, A. B., & Fahey, R. P. 1984, ApJ, 280, 712
Verner, D. A., Verner, E. M., & Ferland, G. J. 1996, At. Data Nucl. Data Tables, 64, 1
Wang, Y.-M., et al. 1998, ApJ, 498, L165
Woods, D. T., Klein, R. I., Castor, J. I., McKee, C. F., & Bell, J. B. 1996, ApJ, 461, 767